# Textural-Structural Joint Learning for No-Reference Super-Resolution Image Quality Assessment

Yuqing Liu, Qi Jia, Shanshe Wang, Siwei Ma Senior Member, IEEE, Wen Gao Fellow, IEEE,

Abstract-Image super-resolution (SR) has been widely investigated in recent years. However, it is challenging to fairly estimate the performances of various SR methods, as the lack of reliable and accurate criteria for perceptual quality. Existing SR image quality assessment (IQA) metrics usually concentrate on the specific kind of degradation without distinguishing the visual sensitive areas, which have no adaptive ability to describe the diverse SR degeneration situations. In this paper, we focus on the textural and structural degradation of image SR which acts as a critical role for visual perception, and design a dual stream network to jointly explore the textural and structural information for quality prediction, dubbed TSNet. By mimicking the human vision system (HVS) that pays more attention to the significant areas of the image, we develop the spatial attention mechanism to make the visual-sensitive areas more distinguishable, which improves the prediction accuracy. Feature normalization (F-Norm) is also developed to investigate the inherent spatial correlation of SR features and boost the network representation capacity. Experimental results show the proposed TSNet predicts the visual quality more accurate than the state-ofthe-art IQA methods, and demonstrates better consistency with the human's perspective. The source code will be made available at http://github.com/yuqing-liu-dut/NRIQA\_SR.

Index Terms—No-reference image quality assessment, convolutional neural network, image super-resolution, attention mechanism, feature normalization, human vision system.

#### I. INTRODUCTION

ITH the rapid development of high-definition display technologies, image super-resolution (SR) has been widely investigated in advanced applications, which aims to generate high-resolution (HR) images from given low-resolution (LR) instances. Although there are numerous image SR works in the past years, how to estimate the quality of super-resolved images still remains challenging.

There are special textural and structural degradation situations in SR processing, making it hard to accurately predict the perceptual quality [1]. According to the human vision system (HVS), the textural and structural degeneration is essential to the visual experience [2]. General image quality assessment (IQA) metrics are usually developed for the simulated signal

Y. Liu is with the School of Software, Dalian University of Technology, Dalian 116620, China (e-mail:liuyuqing@mail.dlut.edu.cn).

Corresponding author: Siwei Ma



Original Image (PSNR/SSIM/TSNet)

Noise Image (18.07/0.6717/0.6330)



Blurred Image (23.01/0.6611/0.2852)

SR Image (23.82/0.7097/0.5146)

Fig. 1. Comparisons among different IQA metrics. (a) original image. (b) noise image. (c) blurred image. (d) super-resolved image. The higher prediction score denotes the better quality. The proposed SR IQA method (TSNet) describes the image quality more in consistence with the visual experience.

degradation and random noise, which are in low correlation with the subjective perspective of SR images. In Figure 1, we can find that the SR image removes the noise and blur and gets higher PSNR [3] and SSIM [4] scores. However, the over-smoothed and sharped SR image losses the textural and structural information and decreases the visual quality. In this point of view, SR IQA metrics are more suitable for visual quality prediction [5]–[8].

Most of the recent no-reference (NR) IQA methods for SR images usually focus on only one kind of the degradation, which limits the representation of information loss. There are different hand-crafted extractors to describe the textural features, such as the local/global frequency features [9], spatial principal component analysis (PCA) features [10], and the mean subtracted contrast normalized (MSCN) coefficients [11]. The textural features are used for evaluating the difference between the SR images and the natural images by natural scene statistics (NSS). However, it is difficult to

Q. Jia is with International School of Information Science and Engineering, Dalian University of Technology, Dalian 116620, China (e-mail: jiaqi@dlut.edu.cn).

S. Wang, S. Ma, and W. Gao are with the School of Electronics Engineering and Computer Science, Institute of Digital Media, Peking University, Beijing 100871, China (e-mail: sswang@pku.edu.cn; swma@pku.edu.cn; wgao@pku.edu.cn)

describe the structural degradation by the pixel-wise statistical analysis. There is also work utilizing the CNN-based feature extractor to explore the perceptual information for mean opinion score (MOS) regression [12]. The pre-trained deep CNN holds effective capacity for structural feature exploration, but lacks to describe the textural degradation by the high-level feature representation [13]. Recently, KLTSRQA [14] utilizes Karhunen-Loéve Transform (KLT) to separate the structural and textural information and regresses the MOS. However, the hand-crafted extractors have no adaptive ability to learn the diverse SR features and limits the accuracy.

The key issue of NR-IQA is to build a metric that in consistence with the human vision system (HVS). According to the HVS, different areas of the images hold different importance for visual perception [15]. However, recent NR-IQA methods usually neglect to distinguish the visual sensitive information in the image, which restricts the effectiveness of prediction. The NSS-based SR metrics usually take the image as a whole without the consideration of saliency detection. Recent CNN-based NR-IQA metrics for image SR treat different areas of the image equally [16]–[18], which have no ability to highlight the visual sensitive information for MOS prediction.

In this paper, we design an end-to-end dual stream network to jointly explore the textural and structural features from the image, dubbed TSNet, for NR-IQA. One VGG-based [19] branch is designed for perceptual structural information extraction [13]. Another CNN branch is developed to explore the pixel-wise textural information with shallow layer extractors [13]. By mimicking the HVS [15] that pays more attention to the significant information, spatial attention mechanism is introduced to make the visual sensitive areas more distinguishable. Furthermore, feature normalization (F-Norm) is also developed to investigate the inherent spatial correlation of SR features [20], [21]. Experimental results show the proposed TSNet predicts the perceptual score more accurately than state-of-the-art IQA methods, and demonstrates better consistency with the human's perspective, as shown in Figure 1.

Our contributions can be concluded as follows:

- We design an end-to-end dual stream network named TSNet for NR-IQA on SR images, which jointly explores the textural and structural information for visual perception.
- We utilize spatial attention mechanism to emphasize the significant information, resulting the visual sensitive areas more distinguishable.
- Experimental results show the proposed TSNet is more consist with the human's perspective than state-of-the-art IQA methods, rendering the accurate prediction of the subjective quality.

# II. RELATED WORKS

# A. Image Super-Resolution

Image super-resolution (SR) is a classical topic in computer vision area. The task of image SR is to generate a high-resolution (HR) image from the given low-resolution (LR) instance. Traditional image SR methods usually upscale the image by interpolation [22] or dictionary learning [23]. The

generated textures vary a lot due to the different technologies and training datasets [24]. As such, it is difficult to model the degeneration of SR step by simply combining the handcrafted signal losses. Recently, deep learning has demonstrated its amazing performance on image SR. SRCNN [25] is the first convolutional neural network (CNN) based method for image SR. After that, VDSR [26], EDSR [27], and other works achieve great success on reconstructing the HR images. These works aim to build a reliable result and choose mean average error (MAE) or mean square error (MSE) as the loss function, which product unnatural results with higher PSNR/SSIM scores and lower perceptual qualities [28]. Generative adversarial networks (GANs) have also been considered in image SR area for generating images with higher visual quality. SRGAN [28], ESRGAN [29] and other works have shown superior performances on restoring satisfying results but the objective scores are lower. Due to the diversity of SR technologies, it is challenging to find a reliable and accurate metric for estimating the restored images.

# B. General Image Quality Assessment

Image quality assessment (IQA) has been widely investigated in recent years. The task of IQA is to design a metric consist with the human's perspective and accurately estimate the image quality. General IQA aims to measure specific types of degradation or their combinations, such as ringing effect, blocking artifacts, blur and noise [30]. IQA can be generally divided into three categories: full-reference (FR) IQA, reduced-reference (RR) IQA and no-reference (NR) IOA. PSNR [3] and SSIM [4] are two most famous FR-IOA metrics that widely used in different applications. Although they can successfully describe the difference between original and distorted images, the objective metrics are not highly correlated with the subjective opinion. Based on PSNR/SSIM, there are variants to better illustrate the image quality, such as PSNR-HVS [31], MS-SSIM [32] and CW-SSIM [33]. GMSD provided a new perspective to evaluate the image quality based on the gradient magnitude similarity deviation [34]. VIF studied the human vision system (HVS) and estimated the image quality by visual information fidelity [35]. Recently there are CNN-based FR-IQA methods achieving accurate performance. PieAPP [36] developed a deep CNNbased network to assess the perceptual image error between the referenced and distorted images. LPIPS [37] utilized a VGG-based encoder to extract the image feature and calculated the distance between different images. DISTS [38] observed the influence of structure and texture similarity on HVS, and proposed a CNN-based image quality metric. Although these works can good describe the subjective difference between the referenced and distorted images, the FR-IQA metrics require original high quality images which may not be accessible in practical situations.

NR-IQA gets more and more attentions in recent years because of the flexibly. NR-IQA metrics usually rely on the hand-crafted extractors or CNN-based architectures to explore the image features and predict the human's perspective [39]. NIQE [40] built a space domain natural scene statistic model

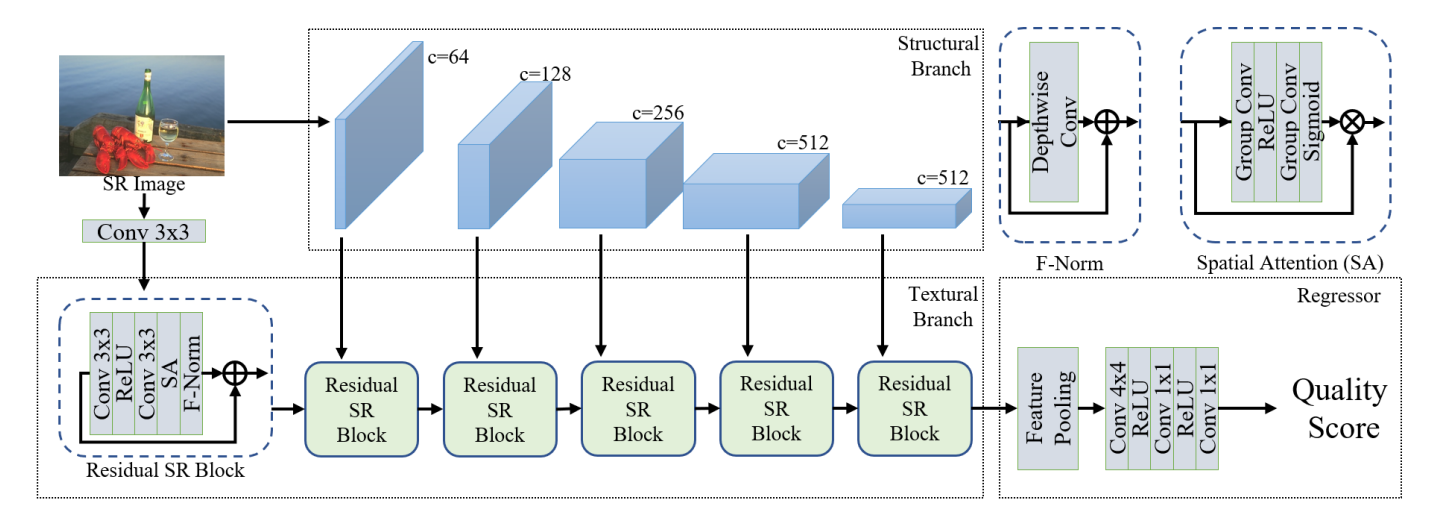


Fig. 2. The architecture of TSNet. The structural branch utilizes a VGG-19 extractor to explore the structural information. The textural branch stacks the proposed residual SR blocks to explore the textural information.

and provided an opinion-free indicator to estimate the subjective quality. BRISQUE [41] assessed the naturalness of images that consists with the visual perception. Recently, CNN-based metrics also demonstrate good performances on NR-IQA. Kang et al. used convolutional and pooling layers to explore the features and fit the perceptual score [42]. NIMA [43] developed a network with the help of classification backbones and regressed the quality score. Su et al. proposed a self-adaptive hyper network (HyperIQA) for blind IQA with good performance [44]. DBCNN [45] provided a dual bilinear network for NR-IQA. MUSIQ [46] also developed a transformer-based NR-IQA metric for the multi-scale information. Despite there are numerous NR-IOA methods with well-designed extractors and regressors, they almost neglect to investigate the special textural and structural degradation caused by image SR.

# C. Image Quality Assessment for Image Super-Resolution

Different from General IQA, there are special textural and structural degradation situations in SR, making it hard to accurately predict the image quality. Ma *et al.* devised a NR-IQA method to regress the perceptual quality of SR images [9]. Jiang *et al.* provided a new perceptive on SR metric by splitting the structural and textural information with Karhunen-Loéve Transformation [14]. Zhang *et al.* integrated AdaBoost decision tree regression and ridge regression to predict the quality score [10]. Zhou *et al.* provided a hand-crafted similarity estimator for FR-IQA on SR images [5]. Berón *et al.* built an opinion-free NR-IQA metric with the help of optimally extracted perceptual features [47]. These works highly rely on the hand-crafted extractors, which limit the representation capacity of features.

There are also CNN-based SR IQA metrics. Ahn *et al.* observed the influence of different distortion models, and developed a deep learning-based distortion sensitivity FR-IQA network for SR images [48]. Zhao *et al.* devised a dual stream network to predict the image quality with the help of LR images [1]. Zhang *et al.* also provided a NR-IQA metric with

the help of VGG feature extractor [12]. However, these works almost neglect to distinguish the special degradation of SR images, and just utilize general CNN architectures to predict the opinion score.

#### III. METHODOLOGY

In this section, we introduce the proposed textural-structural joint learning network (TSNet) in the following manner. We introduce the prediction pipeline firstly. Then, we discuss the block design of the network with feature normalization (F-Norm) and the spatial attention (SA) mechanism, which are specially designed for SR features. Finally, the implementation details are described particularly.

#### A. Prediction Pipeline

Given a SR image  $I^{SR}$ , the task of NR-IQA is to predict the perceptual quality score  $Q_{score}$  by a network such that

$$Q_{score} = TSNet(\mathbf{I}^{SR}), \tag{1}$$

where  $TSNet(\cdot)$  denotes the proposed TSNet.

Figure 2 shows the design of TSNet. The network is composed of the extractor and the regressor. The extractor explore the textural and structural features by two dual branches. After exploration, the regressor predicts the quality score by the non-linear mapping design. There are two branches in the extractor. The structural branch extracts the high-level semantic information by a pretrained VGG-19 extractor [13], [19]. Let  $\mathbf{F}^S$  be the structural features, then there is

$$\{\mathbf{F}_i^S\}_{i=1}^5 = VGG(\mathbf{I}^{SR}),\tag{2}$$

where  $\mathbf{F}_i^S$  is the *i*-th structural feature explored by the VGG-19 extractor. The channel numbers of extracted features are with c=64,128,256,512 and 512 separately, and the resolutions of features are halved progressively.

Correspondingly, there are stages in the textural branch to explore the low-level textural information and mix the structural features by the designed residual SR block. Let  $\mathbf{F}^T$ 

0.9673

0.9690

0.9711

0.9720

0.9649

0.9662

0.9689

0.9702

w/o

w/o

w/o

w

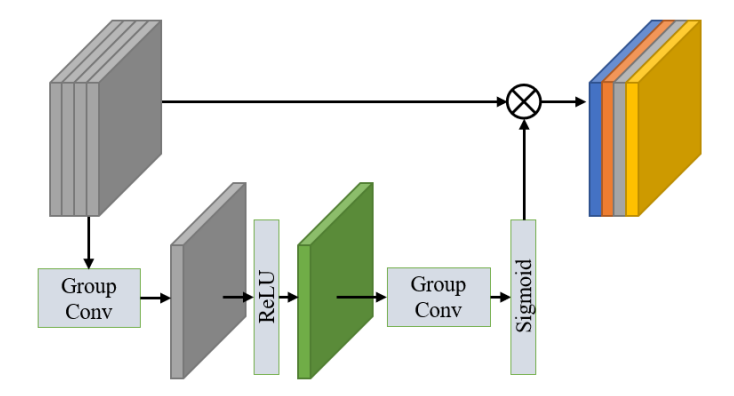


Fig. 3. Design of Spatial Attention (SA).

be the explored textural feature, then for the i-th stage in the textural branch, there is

$$\mathbf{F}_{i}^{T} = RSRB([\mathbf{F}_{i-1}^{S}, \mathbf{F}_{i-1}^{T}]), \tag{3}$$

where  $RSRB(\cdot)$  is the designed residual SR block, and  $[\cdot]$  denotes the channel concatenation operation. To keep the same resolution as  $\mathbf{F}^S$ , there is a max-pooling operation on  $\mathbf{F}^T$  after each stage.

For the first stage of  $\mathbf{F}^T$ , we utilize one convolutional layer and one residual SR block to explore the features from  $\mathbf{I}^{SR}$ , that is

$$\mathbf{F}_{1}^{T} = RSRB(Conv(\mathbf{I}^{SR})). \tag{4}$$

After exploration, the regressor predicts the quality score from the extracted features. There are 6 stages in the textural branch, then the quality score is predicted as

$$Q_{score} = Reg(\mathbf{F}_6^T), \tag{5}$$

where  $Reg(\cdot)$  is the regressor.

#### B. Residual SR Block

As shown in Figure 2, the residual SR block is composed of two convolutional layers, one ReLU activation, one SA layer and one F-Norm. The residual SR block follows the design in recent SR works [20], [27], [29] and removes the batch normalization. The SA layer and the F-Norm are developed at the end of residual SR block, following the recent network designs [20], [49], [50].

In the block, SA layer is utilized to make the important information more distinguishable by mimicking the human vision system (HVS) [15], which is composed of two group convolutional layers, one ReLU activation and one Sigmoid activation. Figure 3 shows the design of SA layer. One group convolution processes the input feature maps with group number as  $c_{sa}/4$ , where  $c_{sa}$  is the channel number of the input feature of SA. There are  $c_{sa}/4$  filters in the group convolution. After that, one ReLU activation processes the feature to introduce the non-linearity. One symmetrical group convolution restores the shape of feature with filter number as  $c_{sa}$  and group number as  $c_{sa}/4$ . A Sigmoid activation is used to make the attention no-negative.

Besides the SA layer, F-Norm [20] is also developed in the residual SR block to substitute the batch normalization. The upper right of Figure 2 shows the design of F-Norm. The F-Norm is composed of one depth-wise convolutional layer and one residual connection. Different from the batch normalization that widely used in different works [28], [45], F-Norm is more suitable for SR features since it can avoid the texture confusion and save the memory cost [20].

# C. Implementation Details

The structural branch of the TSNet is implementated by a pretrained VGG-19 network architecture. The five features are from layers with number l=2,7,12,21, and 30. The textural branch of the TSNet is composed of six residual SR blocks. All convolutional layers in the residual SR blocks are with filter number as f=64 and the kernel size as  $3\times 3$ , except for the SA layer.

The regressor uses feature pooling to embed the features and utilizes convolutional layers to regress the quality score. Adaptive max pooling and adaptive average pooling methods compress the feature maps with size  $4\times 4$ . Then, the convolutional layers in the regressor process the compressed features with filter number as f=256,64 and 1 separately. There is no padding in the convolutional layers, such that the regressor can generate the quality score from features with any resolution.

### IV. EXPERIMENT

## A. Settings

We choose two widely used SR-IQA datasets (CVIU-17 [9] and QADS [2]) for training and testing our TSNet. CVIU-17 [9] proposed by Ma et al. is one of the famous NR-IQA dataset for SR images, which contains 1620 images generated by nine traditional and CNN-based methods from six scaling factors. We randomly choose 60% images for training, 20% for validation and 20% for testing. QADS is also a famous FR-IQA dataset with 980 SR images, which specially contains the results from the GAN-based method. We use the same strategy as CVIU-17 to split the dataset for training and testing. We update the TSNet for 100 epochs by Adam optimizer [51] with learning rate as  $lr = 10^{-4}$ . The network is implemented by the PyTorch [52] platform, and trained on one NVIDIA GTX 3080-Ti GPU. The performances of different methods are estimated by Pearson's linear correlation coefficient [53] (PLCC) and Spearman's rank correlation coefficient [54] (SRCC). The loss function is chosen as  $\ell_1$  loss between the prediction result and the mean opinion score (MOS).

#### B. Model Analysis

1) Investigation on F-Norm and SA: To investigate the effectiveness of F-Norm and SA, we compare the PLCC and

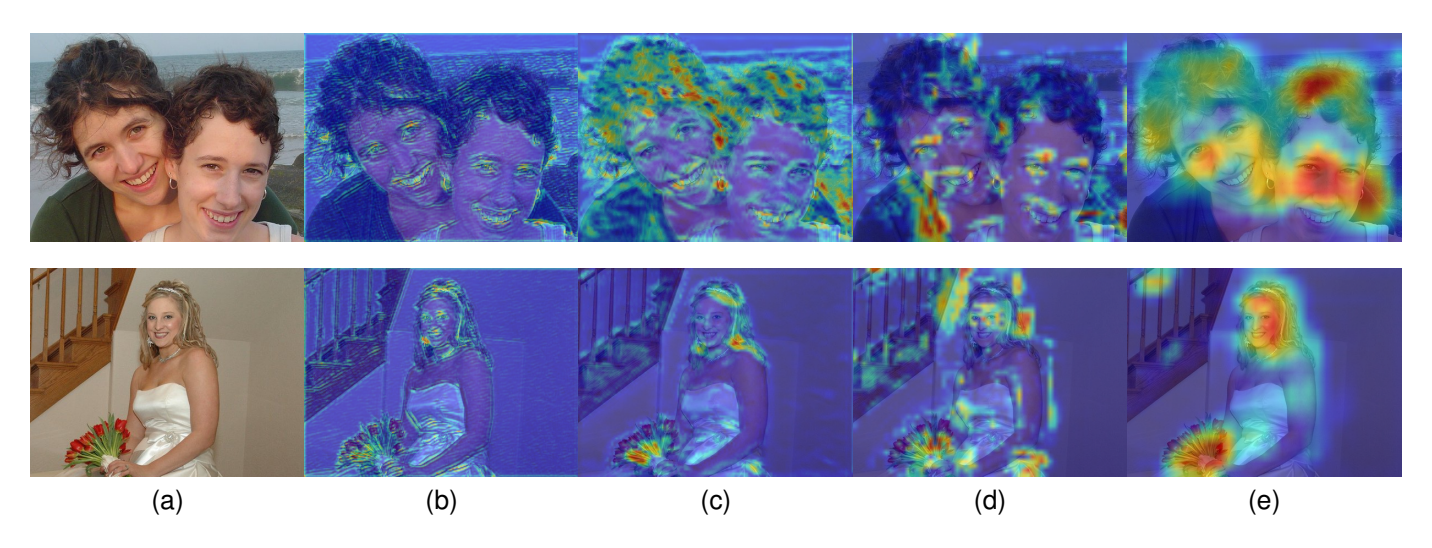


Fig. 4. Visualized attention maps of different images. (a) input image. (b)-(e) the learned attention from stage i=3 to 6. All of the attentions are normalized in range 0 to 1. The red areas mean the higher attention values, and the blue areas means the lower attention values. The visual sensitive areas become more distinguishable with the increase of stages.

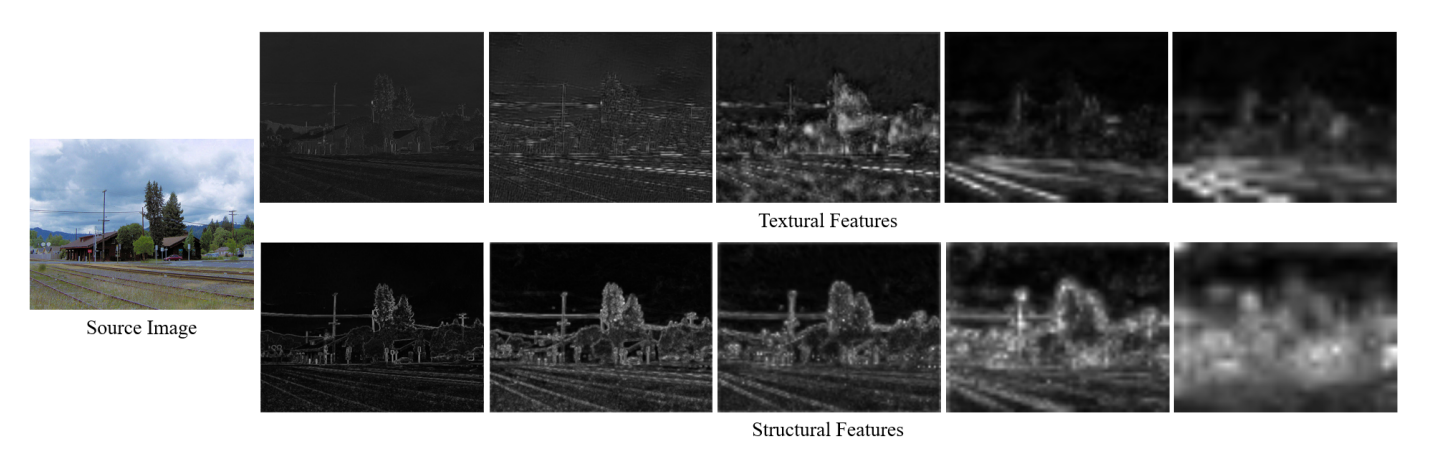


Fig. 5. Visualized features from textural and structural branches. The upper side images are explored textural features from stage i=1 to 5. The lower side images are explored structural features from corresponding stages.

SRCC on the QADS dataset. Table I shows the performance comparisons between F-Norm and SA on QADS dataset. In the table, we can find that the model with both F-Norm and SA achieves the highest PLCC and SRCC results than other methods. According to the results with and without SA (first and second lines), the SA brings 0.002 improvement on both PLCC and SRCC. From the results with and without F-Norm (first and third lines), the F-Norm leads to near 0.004 improvement on PLCC and 0.004 on SRCC. Specially, we can find from the results that F-Norm is more effective than SA with better PLCC/SRCC result. In this point of view, the F-Norm and SA boost the network performance and make the prediction more consist with the human's perspective.

The SA is designed to make the visual sensitive features more distinguishable. To address this point, we illustrate and demonstrate the learned attention. Figure 4 shows the visualized attention maps of different images. The (a) column denotes the original input image, and the (b)-(e) columns are the learned attention maps from stage i=3 to 6, which are normalized in range 0 to 1. The red area means the higher

value, and the blue area means the lower value. From the upper images of the figure, we can find that the complex textures become noticeable at the second stage, such as the hairs, mouths, and canthus. With the increase of stages, the attention concentrates more on the hairs and faces. We can find in the attention map of stage 6 that the eyes and haris become noticeable with a significant higher attention value. This is in accordance with the human vision system (HVS) that people usually pay attention to the faces in the picture. The similar situation can be observed in the lower images of the figure. We can find that at the stage 3, some complex textures are observed with different attention values. With the increase of stages, the face and the flower become more distinguishable, which are more sensitive to the HVS.

2) Investigation on the structural and textural extraction: In the network, we devise two branches to explore the structural and textural features. To show the effectiveness of the dual exploration, we compare the performances of models with different branches. Table II shows the PLCC/SRCC performance comparisons between structural and textural branches

TABLE II
PLCC/SRCC PERFORMANCE COMPARISONS BETWEEN STRUCTURAL AND
TEXTURAL BRANCHES ON QADS DATASET.

Structural	Textural	PLCC ↑	SRCC ↑
w/o	w/o	0.8946	0.8883
w/o	w	0.9587	0.9568
w	w/o	0.9704	0.9691
w	w	0.9720	0.9702

on QADS dataset. The model only with textural branch means that no VGG-19 feature is developed. The model only with structural branch means that we only consider the features from VGG-19 and stacks residual SR blocks to explore the structural information. The model without any branch means that only one  $3\times 3$  convolutional layer extracts the features from the image, and the regressor predicts the score from the feature maps. In the table, we can find that the structural branch brings 0.08 PLCC and SRCC improvement when compared with model without any branch. Similarly, the textural branch brings 0.06 PLCC/SRCC improvement. By combing the structural and textural branches, the model achieves the best performance than other situations.

Figure 5 shows the visualized textural and structural features from different stages. The left side of the figure is the source image. The upper side images of the figure are explored textural features from stages i = 1 to 5, and the lower side images are corresponding structural features. In the figure, we can find that the textural features have higher response on the grass and the tree, which contain more complex textural information. Correspondingly, the structural features have higher response on the contour of the tree and the lines in the picture. Furthermore, with the increase of stages, we can find that the response on sky becomes lower on the textural features while it becomes higher on the structural features. This is because that there are few textures on the cloud, while the edges of the cloud are clear. This observation is in accordance with our motivation that the VGG extractor explores the structural information, while the residual SR blocks explore the textural information.

#### C. Comparison with State-of-the-Art Methods

We compare our model with 10 FR-IQA methods: PSNR [3], SSIM [4], MS-SSIM [32], GMSD [34], FSIM [55], VIF [35], VSI [56], LPIPS [37], PieAPP [36], and DISTS [38]. We also compare our model with 7 NR-IQA methods: CNNIQA [42], HyperNet [44], DBCNN [45], NIQE [40], NIMA [43], BRISQUE [41] and WaDIQaM [57]. Specially, we compare our method with two SR-IQA metric: NRQM [9] and SFSN [5]. NIQE and BRISQUE are calculated by the MATLAB built-in function. NRQM and SFSN are calculated by the official code. We use the provided weight of NRQM for testing without further finetuning. Other implementations follow the GitHub repository<sup>1</sup>. For a fair comparison, we re-train the CNNIQA, HyperNet, WaDIQaM, NIMA and DBCNN under the same protocol according to our method. Specially, the images predicted by HyperNet are resized as  $224 \times 224$ 

TABLE III
PLCC/SRCC COMPARISONS ON QADS DATASET AMONG DIFFERENT
METHODS

Type	Method	PLCC	SRCC
	PSNR [3]	0.3099	0.3260
	SSIM [4]	0.5187	0.5378
	MS-SSIM [32]	0.6586	0.7582
	GMSD [34]	0.7694	0.7988
Full Ref	FSIM [55]	0.6700	0.6951
run Kei	VIF [35]	0.8286	0.8394
	VSI [56]	0.5402	0.5850
	LPIPS [37]	0.6775	0.6782
	PieAPP [36]	0.7481	0.8525
	DISTS [38]	0.6739	0.6711
	NIQE [40]	0.0939	0.0783
	BRISQUE [41]	0.5864	0.6172
No Ref	CNNIQA [42]*	0.9105	0.9034
	HyperNet [44]*	0.8413	0.8375
	DBCNN [45]*	0.9477	0.9453
	NRQM [9]	0.7209	0.7231
SR Metrics	SFSN [5]	0.7590	0.8685
	TSNet(Ours)	0.9720	0.9703

for training and testing, which follows the requirement of the model's implementation. The FR-IQA methods are not fine-tuned on the datasets for a fair comparison, sicne we cannot access the HR images during the no-reference assessment.

Table III shows the PLCC/SRCC comparisons on QADS dataset among different IQA methods. The FR-IQA methods are tested with the original model weights. The starred methods are re-trained on the QADS dataset. We can find that our method achieves the best PLCC/SRCC results than other works. Compared with CNNIQA, HyperNet and DBCNN that retrained under the same protocol, our method achieves 0.1 improvement on PLCC and SRCC. Specially, NRQM and SFSN are specially designed for SR assessment. NRQM is a NR-IQA metric and SFSN is a FR-IQA method. Compared with these works, our method demonstrates a significant superior performance that more consist with the human's perspective.

In the table, we can also find that the general IQA methods usually perform no better than the SR-IQA methods. This is in accordance with our motivation that the general methods usually focus on the hand-crafted signal degradation and noise, but rarely investigate the special textural and structural degradation in the SR situation.

Besides QADS, we also compare the performance on CVIU-17 dataset. Table IV shows the PLCC/SRCC comparisons on CVIU-17 dataset. We can find that our method achieves the best performance than other works, which means the predicted scores of TSNet are more consist with the human's perspective. The starred methods are re-trained under the same protocol of our method. Compared with DBCNN and NIMA, the TSNet achieves 0.01 improvement on PLCC and SRCC. The FR-IQA methods perform better on the CVIU-17 dataset than the QADS dataset, since there are fewer CNN-based methods in CVIU-17. Even though, our method achieves much better PLCC/SRCC result than the FR-IQA methods. We do not compare TSNet with NRQM since the training data of its official model has an intersection with our testing images. Even though, our method leads to a large improvement than SFSN, which is a state-of-the-art FR-IQA method for SR

<sup>&</sup>lt;sup>1</sup>https://github.com/chaofengc/IQA-PyTorch

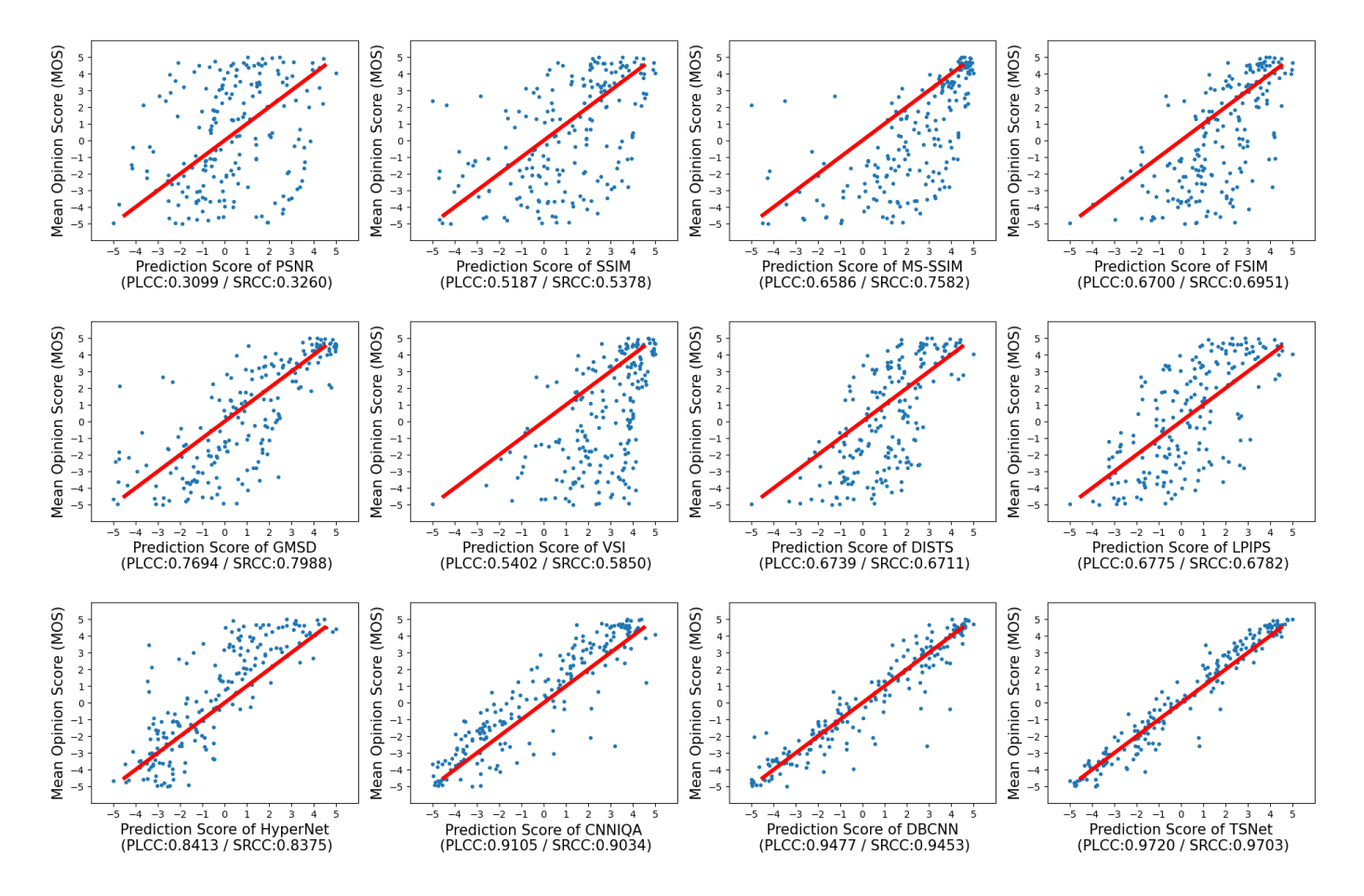


Fig. 6. Scatter plots of different IQA methods on QADS dataset. The blue points denote the testing instances. The red line is the ideal linear relationship between MOS and the prediction score. All of the values are normalized in range -5 to 5 for better view. The result of TSNet has the highest linear correlation with MOS, which means TSNet is the most consist with the human's perspective.

TABLE IV
PLCC/SRCC COMPARISONS ON CVIU-17 DATASET AMONG DIFFERENT
METHODS

Type	Method	PLCC	SRCC	
	PSNR [3]	0.5985	0.5659	
	SSIM [4]	0.6322	0.6249	
	MS-SSIM [32]	0.7452	0.8089	
	GMSD [34]	0.8359	0.8580	
Full Ref	FSIM [55]	0.7504	0.7678	
run Kei	VIF [35]	0.8453	0.8660	
	VSI [56]	0.6969	0.7249	
	LPIPS [37]	0.8306	0.8220	
	PieAPP [36]	0.7841	0.7832	
	DISTS [38]	0.8642	0.8643	
	NIQE [40]	0.3150	0.3279	
	BRISQUE [41]	0.2130	0.2277	
	NIMA [43]*	0.9601	0.9558	
No Ref	CNNIQA [42]*	0.9280	0.9177	
	HyperNet [44]*	0.8863	0.8836	
	DBCNN [45]*	0.9659	0.9602	
	WaDIQaM [57]*	0.9254	0.9185	
SR Metrics	SFSN [5]	0.7547	0.8612	
SK WIELICS	TSNet(Ours)	0.9741	0.9720	

images.

To further investigate the effectiveness of the proposed TSNet, we demonstrate the scatter plots between the MOS and the prediction scores and analyze the correlation. Fig-

ure 6 shows the scatter plots of different IQA methods on QADS dataset. The red line shows the ideal linear relationship between MOS and prediction results. All of the values are normalized in range -5 to 5 for better view. The first and second rows are FR-IQA methods. The methods in the last row are retrained CNN-based NR-IQA works and our TSNet. In the figure, we can find that results of TSNet are more in line with the MOS. Compared with CNNIQA and DBCNN, there are fewer outliers in the TSNet. Figure 7 shows the scatter plots on CVIU-17 dataset. We can find that compared with the FR-IQA methods and the finetuned NR-IQA methods, our TSNet has fewer outliers and performs more consistently with the MOS.

In order to evaluate the effectiveness of TSNet on different SR methods, we also compare the PLCC/SRCC performances on three kinds (interpolation-based, dictionary-based, CNN-based) of SR methods in QADS dataset. Table V shows the results of different IQA metrics on different SR methods. In the table, we can find our method achieves the best performances on all SR methods than other IQA metrics. The images of deep learning SR methods are difficult to predict, since the PLCC/SRCC results are lower than other tasks. Even though, TSNet achieves 0.92 on PLCC and 0.94 on SRCC, which mean the metric is in consistence with the human's

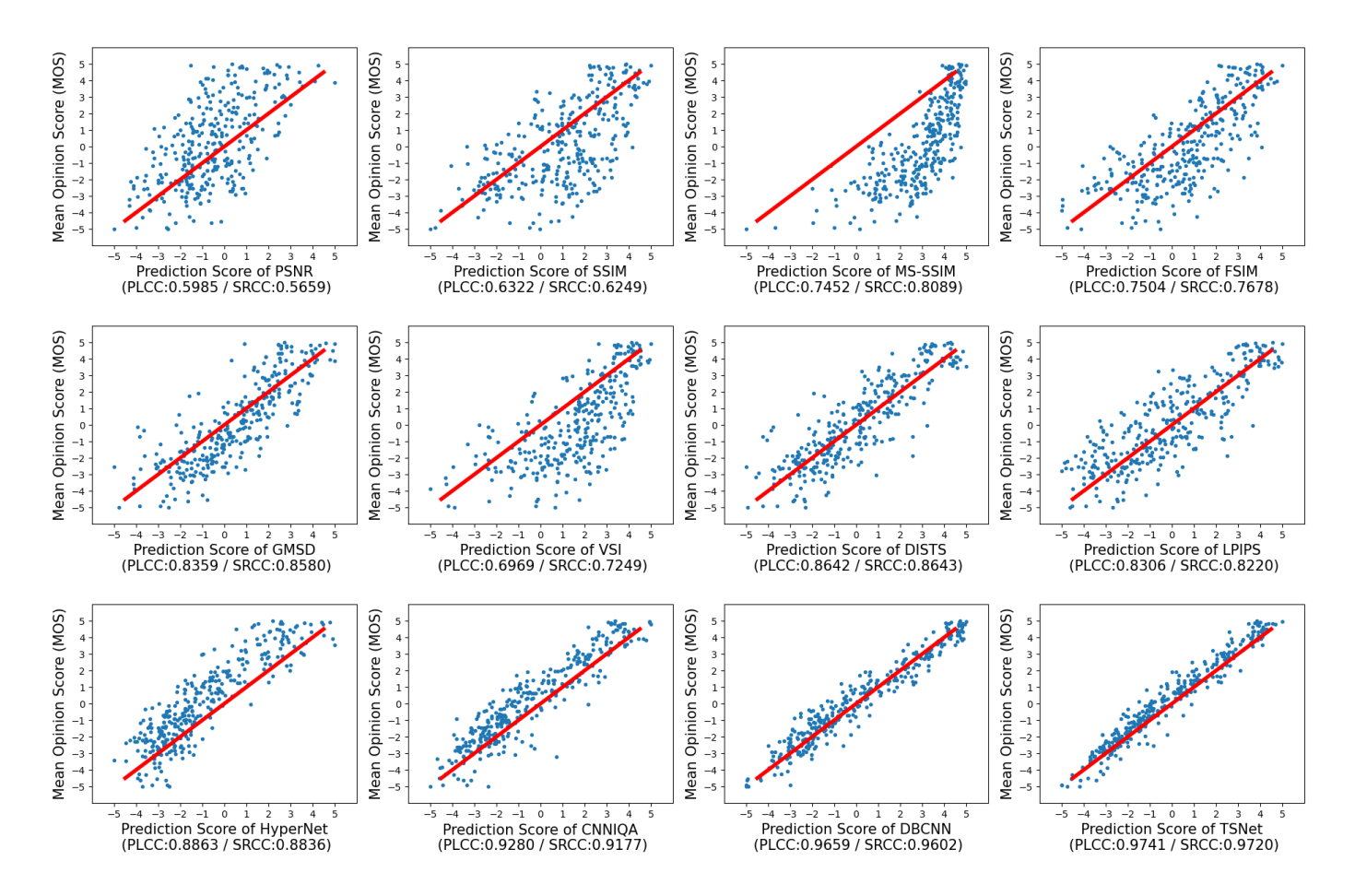


Fig. 7. Scatter plots of different IQA methods on CVIU-17 dataset. The blue points denote the testing instances. The red line is the ideal linear relationship between MOS and the prediction score. All of the values are normalized in range -5 to 5 for better view. The result of TSNet has the highest linear correlation with MOS, which means TSNet is the most consist with the human's perspective.

 $\label{thm:comparisons} TABLE\ V$  PLCC/SRCC comparisons on different SR methods of QADS dataset.

Methods	3	PSNR [3]	SSIM [4]	MS-SSIM [32]	LPIPS [37]	DISTS [38]	DBCNN [45]	CNNIQA [42]	TSNet (Ours)
Interpolation	PLCC	0.0912	0.4710	0.5885	0.6835	0.6812	0.9623	0.9427	0.9730
	SRCC	0.1930	0.4545	0.6076	0.6284	0.6556	0.9374	0.9154	0.9551
Dictionary	PLCC	0.3166	0.5268	0.7211	0.6838	0.6723	0.9478	0.9114	0.9698
	SRCC	0.3195	0.5167	0.7859	0.6728	0.6599	0.9383	0.8812	0.9584
Deep learning	PLCC	0.2005	0.3214	0.4077	0.5308	0.4596	0.7980	0.7339	0.9266
	SRCC	0.2392	0.4143	0.6833	0.5711	0.4832	0.8362	0.7763	0.9455
Total	PLCC	0.3099	0.5188	0.6586	0.6775	0.6739	0.9477	0.9105	0.9720
	SRCC	0.3260	0.5377	0.7582	0.6782	0.6711	0.9453	0.9034	0.9702

## perspective.

To further investigate the statistical significance of the proposed TSNet, we perform the two-sample T-Test [14] on to compare the effectiveness in pairs. We conduct the test by randomly choose 20 images and calculate the SRCC result. The operation is repeated by 20 times, and we can get two distributions from different methods. The T-Test result is calculated between the two SRCC distributions. Figure 8 shows the two-sample T-Test on QADS dataset. 1 in the matrix means that left side method is statistical superior to the upper side one, while -1 means the upper method is better. 0 means the two methods are statistically same. In the figure, we can find that TSNet performs better than all other works. Besides

QADS, Figure 9 shows the T-Test results on CVIU-17 dataset. In the figure we can find that TSNet has the same performance as DBCNN and performs better than all other works. Although the two works are with the statistically same performance, TSNet holds higher PLCC/SRCC results than DBCNN in the Table IV.

#### V. CONCLUSION

In this paper, we proposed a CNN-based NR-IQA method named TSNet. Different from existing NR-IQA methods, we noticed that there are special textural and structural information losses in the SR situation, and devised a dual stream network for joint textural and structural feature exploration.

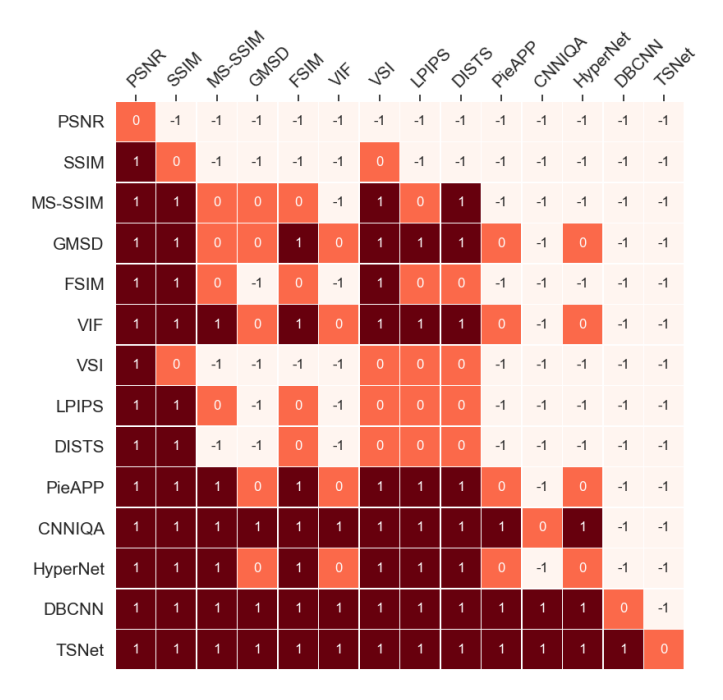


Fig. 8. Two-sample T-Test on QADS dataset. 1 means the left side method is statistical superior to the upper side one, while -1 means the upper method is better. 0 means the two methods are statistically same. TSNet is statistically better than other works with more 1 values on the left.

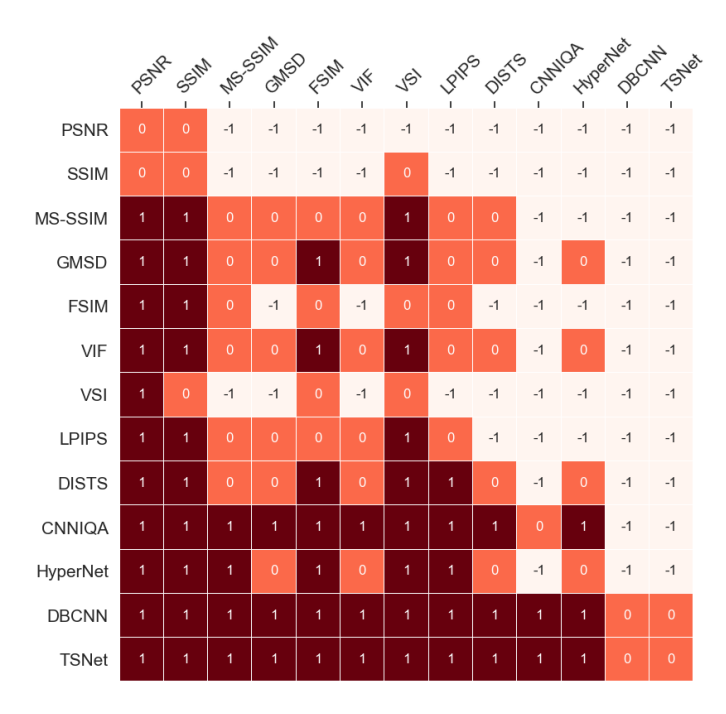


Fig. 9. Two-sample T-Test on CVIU-17 dataset. 1 means the left side method is statistical superior to the upper side one, while -1 means the upper method is better. 0 means the two methods are statistically same. TSNet is statistically better than other works with more 1 values on the left.

Motivated by the human vision system (HVS), we developed the spatial attention mechanism to make the salient information more distinguishable and improve the accuracy of the prediction. Feature normalization (F-Norm) was also considered in the TSNet to better explore the super-resolved features. Experimental results show the proposed TSNet has

achieves better performance on the QADS and CVIU-17 datasets than other state-of-the-art IQA methods.

In future work, we aim to improve the TSNet from three perspectives. Firstly, we decide to design a FR-IQA version of TSNet for better assessment performance. Secondly, we apply the TSNet to image super-resolution tasks, which acts as a loss function for improving the restoration capacity. Finally, we attempt to apply the meta-learning strategy to TSNet, making it more flexible for practical applications.

#### REFERENCES

- T. Zhao, Y. Lin, Y. Xu, W. Chen, and Z. Wang, "Learning-based quality assessment for image super-resolution," *IEEE Transactions on Multimedia*, pp. 1–1, 2021.
- [2] F. Zhou, R. Yao, B. Liu, and G. Qiu, "Visual quality assessment for super-resolved images: Database and method," *IEEE Transactions on Image Processing*, vol. 28, no. 7, pp. 3528–3541, 2019.
- [3] A. Horé and D. Ziou, "Image quality metrics: Psnr vs. ssim," in International Conference on Pattern Recognition (ICPR), 2010, pp. 2366–2369
- [4] Z. Wang, A. Bovik, H. Sheikh, and E. Simoncelli, "Image quality assessment: from error visibility to structural similarity," *IEEE Transactions on Image Processing*, vol. 13, no. 4, pp. 600–612, 2004.
- [5] W. Zhou, Z. Wang, and Z. Chen, "Image super-resolution quality assessment: Structural fidelity versus statistical naturalness," in *International Conference on Quality of Multimedia Experience (QoMEX)*, 2021, pp. 61–64.
- [6] H. Yeganeh, M. Rostami, and Z. Wang, "Objective quality assessment of interpolated natural images," *IEEE Transactions on Image Processing*, vol. 24, no. 11, pp. 4651–4663, 2015.
- [7] J. Chen, Y. Xu, K. Ma, H. Huang, and T. Zhao, "A hybrid quality metric for non-integer image interpolation," in 2018 Tenth International Conference on Quality of Multimedia Experience (QoMEX), 2018, pp. 1–3.
- [8] G. Wang, L. Li, Q. Li, K. Gu, Z. Lu, and J. Qian, "Perceptual evaluation of single-image super-resolution reconstruction," in *IEEE International Conference on Image Processing (ICIP)*, 2017, pp. 3145–3149.
- [9] C. Ma, C.-Y. Yang, X. Yang, and M.-H. Yang, "Learning a no-reference quality metric for single-image super-resolution," *Computer Vision and Image Understanding*, vol. 158, pp. 1–16, 2017.
- [10] K. Zhang, D. Zhu, J. Jing, and X. Gao, "Learning a cascade regression for no-reference super-resolution image quality assessment," in *IEEE International Conference on Image Processing (ICIP)*, 2019, pp. 450–452
- [11] J. Beron, H. D. Benitez-Restrepo, and A. C. Bovik, "Blind image quality assessment for super resolution via optimal feature selection," *IEEE Access*, vol. 8, pp. 143 201–143 218, 2020.
- [12] K. Zhang, D. Zhu, J. Li, X. Gao, F. Gao, and J. Lu, "Learning stacking regression for no-reference super-resolution image quality assessment," *Signal Processing*, vol. 178, p. 107771, 2021.
- [13] J. Johnson, A. Alahi, and L. Fei-Fei, "Perceptual losses for real-time style transfer and super-resolution," in *European Conference on Computer Vision (ECCV)*, B. Leibe, J. Matas, N. Sebe, and M. Welling, Eds., 2016, pp. 694–711.
- [14] Q. Jiang, Z. Liu, K. Gu, F. Shao, X. Zhang, H. Liu, and W. Lin, "Single image super-resolution quality assessment: A real-world dataset, subjective studies, and an objective metric," *IEEE Transactions on Image Processing*, vol. 31, pp. 2279–2294, 2022.
- [15] Q. Lai, S. Khan, Y. Nie, H. Sun, J. Shen, and L. Shao, "Understanding more about human and machine attention in deep neural networks," *IEEE Transactions on Multimedia*, vol. 23, pp. 2086–2099, 2021.
- [16] B. Bare, K. Li, B. Yan, B. Feng, and C. Yao, "A deep learning based no-reference image quality assessment model for single-image superresolution," in *IEEE International Conference on Acoustics, Speech and Signal Processing (ICASSP)*, 2018, pp. 1223–1227.
- [17] Y. Fang, C. Zhang, W. Yang, J. Liu, and Z. Guo, "Blind visual quality assessment for image super-resolution by convolutional neural network," *Multimedia Tools and Applications*, vol. 77, no. 22, pp. 29829–29846, 2018
- [18] V. Khrulkov and A. Babenko, "Neural side-by-side: Predicting human preferences for no-reference super-resolution evaluation," in *Proceedings* of the IEEE/CVF Conference on Computer Vision and Pattern Recognition (CVPR), June 2021, pp. 4988–4997.

- [19] K. Simonyan and A. Zisserman, "Very deep convolutional networks for large-scale image recognition," arXiv preprint arXiv:1409.1556, 2014.
- [20] Y. Liu, S. Wang, J. Zhang, S. Wang, S. Ma, and W. Gao, "Iterative network for image super-resolution," *IEEE Transactions on Multimedia*, pp. 1–1, 2021.
- [21] Y. Liu, Q. Jia, X. Fan, S. Wang, S. Ma, and W. Gao, "Cross-srn: Structure-preserving super-resolution network with cross convolution," *IEEE Transactions on Circuits and Systems for Video Technology*, pp. 1–1, 2021.
- [22] R. Keys, "Cubic convolution interpolation for digital image processing," IEEE Transactions on Acoustics, Speech, and Signal Processing, vol. 29, no. 6, pp. 1153–1160, 1981.
- [23] R. Timofte, V. De Smet, and L. Van Gool, "A+: Adjusted anchored neighborhood regression for fast super-resolution," in *Asian Conference* on Computer Vision (ACCV), D. Cremers, I. Reid, H. Saito, and M.-H. Yang, Eds., 2015, pp. 111–126.
- [24] L. Yue, H. Shen, J. Li, Q. Yuan, H. Zhang, and L. Zhang, "Image superresolution: The techniques, applications, and future," *Signal Processing*, vol. 128, pp. 389–408, 2016.
- [25] C. Dong, C. C. Loy, K. He, and X. Tang, "Image super-resolution using deep convolutional networks," *IEEE Transactions on Pattern Analysis* and Machine Intelligence, vol. 38, no. 2, pp. 295–307, 2016.
- [26] J. Kim, J. K. Lee, and K. M. Lee, "Accurate image super-resolution using very deep convolutional networks," in *IEEE Conference on Computer Vision and Pattern Recognition (CVPR)*, 2016, pp. 1646–1654.
- [27] B. Lim, S. Son, H. Kim, S. Nah, and K. M. Lee, "Enhanced deep residual networks for single image super-resolution," in *IEEE Conference on Computer Vision and Pattern Recognition Workshops (CVPRW)*, 2017, pp. 1132–1140.
- [28] C. Ledig, L. Theis, F. Huszár, J. Caballero, A. Cunningham, A. Acosta, A. Aitken, A. Tejani, J. Totz, Z. Wang, and W. Shi, "Photo-realistic single image super-resolution using a generative adversarial network," in IEEE Conference on Computer Vision and Pattern Recognition (CVPR), 2017, pp. 105–114.
- [29] X. Wang, K. Yu, S. Wu, J. Gu, Y. Liu, C. Dong, Y. Qiao, and C. C. Loy, "Esrgan: Enhanced super-resolution generative adversarial networks," in European Conference on Computer Vision (ECCV). Springer, 2018, pp. 63–79.
- [30] G. Zhai and X. Min, "Perceptual image quality assessment: a survey," *Science China Information Sciences*, vol. 63, no. 11, pp. 1–52, 2020.
- [31] P. Gupta, P. Srivastava, S. Bhardwaj, and V. Bhateja, "A modified psnr metric based on hvs for quality assessment of color images," in *International Conference on Communication and Industrial Application*, 2011, pp. 1–4.
- [32] Z. Wang, E. Simoncelli, and A. Bovik, "Multiscale structural similarity for image quality assessment," in *The Thrity-Seventh Asilomar Confer*ence on Signals, Systems Computers, 2003, vol. 2, 2003, pp. 1398–1402 Vol.2.
- [33] M. P. Sampat, Z. Wang, S. Gupta, A. C. Bovik, and M. K. Markey, "Complex wavelet structural similarity: A new image similarity index," *IEEE Transactions on Image Processing*, vol. 18, no. 11, pp. 2385–2401, 2009.
- [34] W. Xue, L. Zhang, X. Mou, and A. C. Bovik, "Gradient magnitude similarity deviation: A highly efficient perceptual image quality index," *IEEE Transactions on Image Processing*, vol. 23, no. 2, pp. 684–695, 2014.
- [35] H. Sheikh and A. Bovik, "Image information and visual quality," *IEEE Transactions on Image Processing*, vol. 15, no. 2, pp. 430–444, 2006.
- [36] E. Prashnani, H. Cai, Y. Mostofi, and P. Sen, "Pieapp: Perceptual imageerror assessment through pairwise preference," in *IEEE/CVF Conference* on Computer Vision and Pattern Recognition (CVPR), 2018, pp. 1808– 1817.
- [37] R. Zhang, P. Isola, A. A. Efros, E. Shechtman, and O. Wang, "The unreasonable effectiveness of deep features as a perceptual metric," in IEEE/CVF Conference on Computer Vision and Pattern Recognition (CVPR), 2018, pp. 586–595.
- [38] K. Ding, K. Ma, S. Wang, and E. P. Simoncelli, "Image quality assessment: Unifying structure and texture similarity," *IEEE Transactions on Pattern Analysis and Machine Intelligence*, vol. 44, no. 5, pp. 2567–2581, 2022.
- [39] X. Yang, F. Li, and H. Liu, "A survey of dnn methods for blind image quality assessment," *IEEE Access*, vol. 7, pp. 123788–123806, 2019.
- [40] A. Mittal, R. Soundararajan, and A. C. Bovik, "Making a "completely blind" image quality analyzer," *IEEE Signal Processing Letters*, vol. 20, no. 3, pp. 209–212, 2013.

- [41] A. Mittal, A. K. Moorthy, and A. C. Bovik, "No-reference image quality assessment in the spatial domain," *IEEE Transactions on Image Processing*, vol. 21, no. 12, pp. 4695–4708, 2012.
- [42] L. Kang, P. Ye, Y. Li, and D. Doermann, "Convolutional neural networks for no-reference image quality assessment," in *IEEE Conference on Computer Vision and Pattern Recognition (CVPR)*, 2014, pp. 1733–1740.
- [43] H. Talebi and P. Milanfar, "Nima: Neural image assessment," IEEE Transactions on Image Processing, vol. 27, no. 8, pp. 3998–4011, 2018.
- [44] S. Su, Q. Yan, Y. Zhu, C. Zhang, X. Ge, J. Sun, and Y. Zhang, "Blindly assess image quality in the wild guided by a self-adaptive hyper network," in *IEEE/CVF Conference on Computer Vision and Pattern Recognition (CVPR)*, 2020, pp. 3664–3673.
- [45] W. Zhang, K. Ma, J. Yan, D. Deng, and Z. Wang, "Blind image quality assessment using a deep bilinear convolutional neural network," *IEEE Transactions on Circuits and Systems for Video Technology*, vol. 30, no. 1, pp. 36–47, 2020.
- [46] J. Ke, Q. Wang, Y. Wang, P. Milanfar, and F. Yang, "Musiq: Multi-scale image quality transformer," in *IEEE/CVF International Conference on Computer Vision (ICCV)*, 2021, pp. 5128–5137.
- [47] J. Berón, H. D. B. Restrepo, and A. C. Bovik, "Optimal feature selection for blind super-resolution image quality evaluation," in *IEEE International Conference on Acoustics, Speech and Signal Processing* (ICASSP), 2019, pp. 1842–1846.
- [48] S. Ahn, Y. Choi, and K. Yoon, "Deep learning-based distortion sensitivity prediction for full-reference image quality assessment," in *IEEE/CVF Conference on Computer Vision and Pattern Recognition Workshops* (CVPRW), 2021, pp. 344–353.
- [49] J. Hu, L. Shen, S. Albanie, G. Sun, and E. Wu, "Squeeze-and-excitation networks," *IEEE Transactions on Pattern Analysis and Machine Intelli*gence, vol. 42, no. 8, pp. 2011–2023, 2020.
- [50] Y. Zhang, K. Li, K. Li, L. Wang, B. Zhong, and Y. Fu, "Image superresolution using very deep residual channel attention networks," in European Conference on Computer Vision (ECCV), 2018, pp. 294–310.
- [51] D. P. Kingma and J. Ba, "Adam: A method for stochastic optimization," arXiv preprint arXiv:1412.6980, 2014.
- [52] A. Paszke, S. Gross, F. Massa, A. Lerer, J. Bradbury, G. Chanan, T. Killeen, Z. Lin, N. Gimelshein, L. Antiga, A. Desmaison, A. Kopf, E. Yang, Z. DeVito, M. Raison, A. Tejani, S. Chilamkurthy, B. Steiner, L. Fang, J. Bai, and S. Chintala, "Pytorch: An imperative style, high-performance deep learning library," in *Advances in Neural Information Processing Systems (NeurIPS)*, vol. 32, 2019.
- [53] J. Benesty, J. Chen, Y. Huang, and I. Cohen, "Pearson correlation coefficient," in *Noise reduction in speech processing*. Springer, 2009, pp. 1–4.
- [54] C. Wissler, "The spearman correlation formula," *Science*, vol. 22, no. 558, pp. 309–311, 1905.
- [55] L. Zhang, L. Zhang, X. Mou, and D. Zhang, "Fsim: A feature similarity index for image quality assessment," *IEEE Transactions on Image Processing*, vol. 20, no. 8, pp. 2378–2386, 2011.
- [56] L. Zhang, Y. Shen, and H. Li, "Vsi: A visual saliency-induced index for perceptual image quality assessment," *IEEE Transactions on Image Processing*, vol. 23, no. 10, pp. 4270–4281, 2014.
- [57] S. Bosse, D. Maniry, K.-R. Müller, T. Wiegand, and W. Samek, "Deep neural networks for no-reference and full-reference image quality assessment," *IEEE Transactions on Image Processing*, vol. 27, no. 1, pp. 206–219, 2018.